

Dipolar interactions between field-tuneable, localized emitters in van der Waals heterostructures

Weijie Li[†], Xin Lu[†], Sudipta Dubey, Luka Devenica, and Ajit Srivastava*

Department of Physics, Emory University, Atlanta 30322, Georgia, USA

[†]These authors contributed equally to this work.

*Correspondence to: ajit.srivastava@emory.edu

While photons in free space barely interact, matter can mediate interactions between them resulting in optical nonlinearities. Such interactions at the single-quantum level result in an on-site photon repulsion [1, 2], crucial for photon-based quantum information processing and for realizing strongly interacting many-body states of light [3–7]. Here, we report repulsive dipole-dipole interactions between electric field tuneable, localized interlayer excitons in MoSe₂/WSe₂ heterobilayer. The presence of a single, localized exciton with an out-of-plane, non-oscillating dipole moment increases the energy of the second excitation by ~ 2 meV – an order of magnitude larger than the emission linewidth and corresponding to an inter-dipole distance of ~ 5 nm. At higher excitation power, multi-exciton complexes appear at systematically higher energies. The magnetic field dependence of the emission polarization is consistent with spin-valley singlet nature of the dipolar molecular state. Our finding is an important step towards the creation of excitonic few- and many-body states such as dipolar crystals with spin-valley spinor in van der Waals (vdW) heterostructures.

Optical response in atomically thin layered semiconductors is determined by excitons and other excitonic complexes such as trions and biexcitons which are strongly bound due to increased Coulomb interactions in truly 2D limit [5, 9]. In addition, due to the type-II band alignment in heterobilayer of MoSe₂/WSe₂, an interlayer exciton comprising of an electron in the MoSe₂ layer and hole in the WSe₂ layer is found to be stable and long-lived [4, 10, 11, 13]. As shown in Fig. 1a, due to the spatial separation of electron and hole, the interlayer exciton carries a static, out-of-plane electric dipole moment which allows for the tuning of its energy by an external electric field (E). The orientation of this dipole is fixed by the ordering of MoSe₂ and WSe₂ layers and hence leads to a repulsive interaction between interlayer excitons.

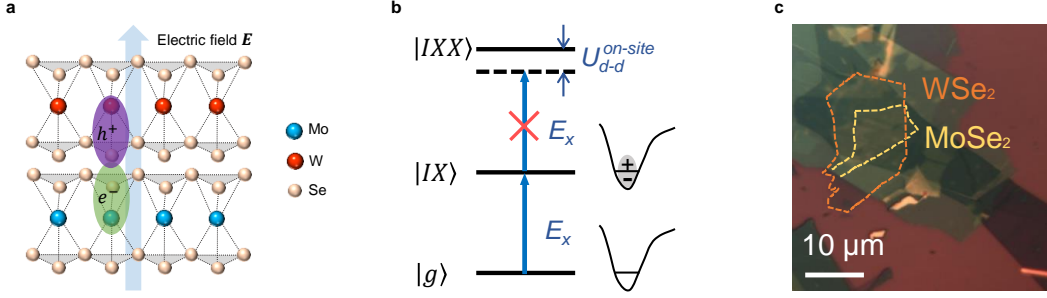


Figure 1: **Interlayer exciton dipoles in WSe₂/MoSe₂ heterostructure.** **a**, A schematic showing the interlayer exciton in WSe₂-MoSe₂ heterobilayer under an external electric field E . Due to the type-II band alignment, electron and hole are separated in MoSe₂ and WSe₂, respectively, forming a permanent out-of-plane dipole. The dipole energy red-shifts (blue-shifts) when E is parallel (anti-parallel) to the direction of dipole. **b**, Energy diagram of localized interlayer exciton and biexciton in a potential well. The energy of biexciton is raised up by on-site dipole-dipole interaction $U_{dd}^{on-site}$. **c**, An optical image of WSe₂/MoSe₂ heterobilayer with graphite bottom gate. Monolayer WSe₂ (MoSe₂) is depicted in orange (yellow) dashed line. The final device has graphite bottom and top gates with h-BN as dielectric on both sides.

This dipolar interaction is potentially interesting for inducing effective photon-photon interaction and making the heterobilayer a nonlinear optical medium for efficient photon switching applications. Furthermore, repulsive dipolar interactions could also lead to exotic many-body states such as self-assembled dipolar crystals with spin-valley degree of freedom at a critical density of excitons [14, 15]. As a signature of nonlinearity, dipolar repulsion should result in an exciton density dependent blueshift of the emission energy with increasing incident power. While such a behavior has been previously reported [16, 17], a discernible shift of the emission energy, comparable to the linewidth, occurs only for a large number of excitons ($\sim 10^4$ - 10^5) and at the highest incident power.

In order to see a quantum nonlinearity where the presence of merely one additional exciton drastically modifies the optical response, the effective dipole-dipole interaction (U_{dd}) must be larger than the linewidth [4]. As the expected blueshift is $U_{dd} \sim 1/r_{ex}^3$ where r_{ex} is the interexcitonic distance, localized interlayer excitons are a good candidate to observe this effect. Localized excitons in monolayer WSe₂ have been shown to be single photon emitters with sharp linewidths [18, 19] and can host a single charge and spin [20, 21]. Very recently, localized interlayer excitons with sharp linewidths were reported in vdW heterostructures [22]. As described in Fig. 1b, there is an

on-site energy cost ($U_{\text{dd}}^{\text{on-site}}$) for creating two interlayer excitons within the same trap ($|IXX\rangle$) compared to a single excitation ($|IX\rangle$) with energy E_X . The situation is then reminiscent of dipole blockade in Rydberg atoms [23] albeit with a much smaller dipole moment and hence requiring tighter localization. In addition to increasing U_{dd} , localized interlayer excitons should also serve as quantum emitters consisting of a single dipole with tuneable emission energy in a perpendicular electric field.

To demonstrate dipole-dipole interactions in localized interlayer excitons, we fabricated a $\text{MoSe}_2/\text{WSe}_2$ heterobilayer encapsulated in hexagonal-boron nitride layers with graphite top and bottom gates, as shown in Fig. 1c (see Methods). Fig. 2a shows the low temperature (~ 4 K) photoluminescence (PL) spectra of our sample with emission from interlayer exciton clearly present at lower energy (~ 1.35 eV) compared to intralayer exciton peaks of MoSe_2 (WSe_2) at 1.65 eV (1.7 eV), consistent with previous studies [24]. Reflectance spectra of the heterobilayer region shown in Fig. 2b exhibits a redshift of intralayer exciton resonances compared to the monolayer regions as is expected from the interaction between the two monolayers [25]. The photoluminescence excitation (PLE) spectroscopy of the lower energy PL peaks shows resonances at excitation energies corresponding to MoSe_2 and WSe_2 excitons, further confirming the interlayer nature of the redshifted peaks (Fig. 2c).

In order to observe localized interlayer excitons, we switch to quasi-resonant excitation close to $\text{MoSe}_2/\text{WSe}_2$ exciton and use low excitation power $\sim \text{nW}$ (Methods). As Fig. 2d shows, we observe sharp, spatially localized peaks with linewidths as low as $110 \mu\text{eV}$ in the energy range of 1260 to 1330 meV (see Supplementary). Furthermore, these sharp emission peaks show spectral jittering which is characteristic of localized quantum emitters. Since the energy of the sharp peaks lies in the range of interlayer PL at higher power and because intralayer WSe_2 and MoSe_2 localized excitons typically exhibit energy higher than 1560 meV [26], we believe that such low-energy peaks should be related to interlayer exciton. To further confirm our claim, we perform PLE spectroscopy and find resonances at both MoSe_2 (~ 1640 meV) and WSe_2 (~ 1730 meV) excitons (Fig. 2e), indicating the interlayer nature of these peaks.

With electron and hole located in different layers due to the type-II band alignment, interlayer exciton has an out-of-plane permanent dipole and its energy should blueshift (redshift) by an amount $\Delta U = -p \cdot \Delta E$ when the electric field (E) is anti-parallel (parallel) to the the direction of dipole p . The dipole moment in our sample is $0.7 \text{ nm} \cdot e$ and points from MoSe_2 (bottom layer)

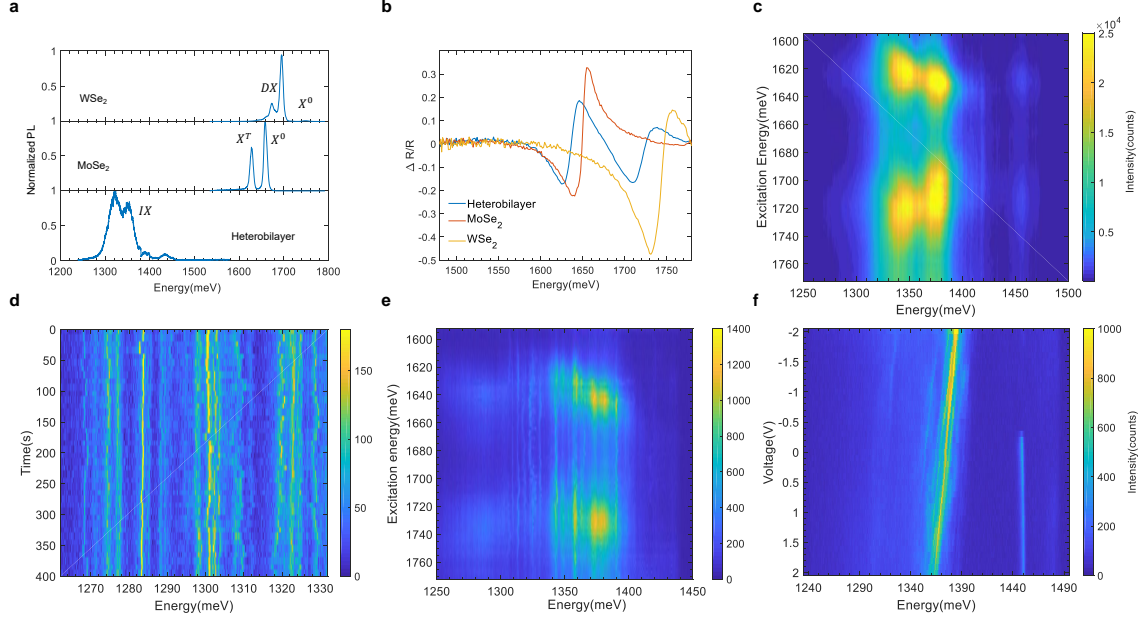


Figure 2: **Excitons from WSe₂/MoSe₂ heterostructure at low temperature (~4 K).** **a**, Normalized photoluminescence (PL) spectra. Top: Emission from defect band (DX) dominates in WSe₂. Exciton X⁰ is observed at ~1750 meV. Middle: Monolayer MoSe₂ shows two prominent peaks at 1658 meV and 1628 meV, corresponding to neutral exciton X⁰ and trion X^T, respectively. Bottom: Emission from interlayer excitons appears at lower energy (1250 - 1450 meV). **b**, Reflectance contrast $\Delta R/R$ spectra. $\Delta R/R = (R_{\text{sample}} - R_{\text{substrate}}) / R_{\text{substrate}}$. The exciton resonances in monolayers are consistent with the observation from PL spectroscopy in panel **a**. Compared to monolayers, the intralayer excitons in heterobilayer red-shift and broaden. **c**, Photoluminescence excitation (PLE) spectroscopy of interlayer excitons. **d**, Time-trace PL emission of localized interlayer excitons. **e**, PLE of localized emitters. All the quantum emitters show local resonances around ~1640 meV (MoSe₂ resonance) and ~1730 meV (WSe₂ resonance), consistent with the nature of interlayer excitons. **f**, Electric field tuning of a localized interlayer exciton. As bottom gate voltage sweeps from -2 to +2 V, the localized interlayer exciton at ~1380 meV exhibits a red-shift of ~20 meV, confirming the existence of an out-of-plane dipole. As a comparison, the localized intralayer exciton at ~1450 meV does not show electric field tunability. Excitation laser is linearly-polarized. Wavelength $\lambda = 633$ nm in panel **a**, $\lambda = 770$ nm in panel **d**, $\lambda = 758$ nm in panel **f**. Incident power $P = 2 \mu\text{W}$, $5 \mu\text{W}$ and $20 \mu\text{W}$ from top to bottom in panel **a**, $P = 10$ nW in panel **d**, $P = 210$ nW in panel **f**.

to WSe₂ (top layer). As the bottom gate voltage changes from -2 to +2 V, ΔE (pointing up) = +4 eV · 80 nm (the estimated thickness between top and bottom gates). We thus expect the energy of interlayer exciton to decrease by ~22 meV. The observed red-shift of ~20 meV (tuning rate of 400 meV nm V⁻¹) in Fig. 2f is in consistent with the analysis [16]. Meanwhile, a localized

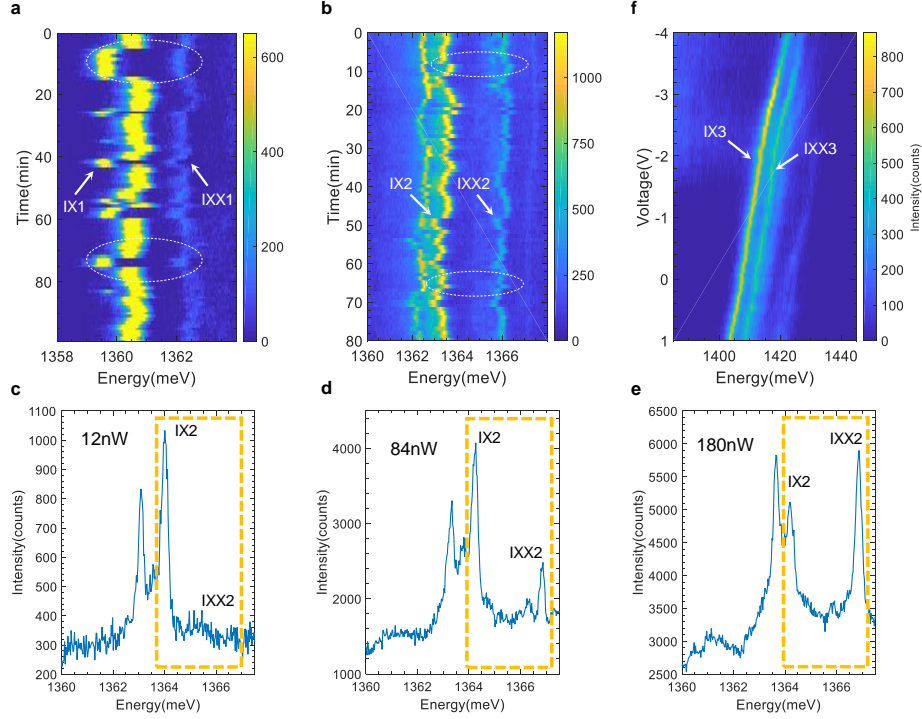


Figure 3: Signature of localized interlayer biexcitons. **a, b,** Time-trace of PL emission of interlayer excitons and biexcitons. White arrows and dotted circles highlight the same spectral jittering patterns from IX1-IXX1 (a) and IX2-IXX2 (b), indicating that they originate from the same quantum emitter. **c-e** PL spectra of IX2-IXX2 under different excitation powers, 12 nW (c), 84 nW (d) and 180 nW (e). Only exciton IX2 shows up at low power (12 nW). Biexciton IXX2 appears at intermediate power (84 nW) and dominates at high power (180 nW). **f,** Electrical tuning of interlayer exciton IX3 and biexciton IXX3. The two peaks exhibit the same tuning rate of $\sim 310 \text{ meV nm V}^{-1}$. Excitation laser is linearly-polarized. Wavelength $\lambda = 745 \text{ nm}$ in panel **a-d**, $\lambda = 758 \text{ nm}$ in panel **f**. Incident power $P = 20 \text{ nW}$ in panel **a**, $P = 250 \text{ nW}$ in panel **b**, $P = 4 \text{ }\mu\text{W}$ in panel **f**.

peak at 1450 meV, possibly from MoSe_2 , hardly shifts with E . This is in agreement with the absence of out-of-plane dipole moment for an intralayer exciton. The E -tunability of sharp peaks unambiguously demonstrates that they arise from localized interlayer excitons. It is very probable that, like their intralayer counterparts, interlayer excitons also get trapped in shallow potentials due to strain or defect potential on a length scale larger than interlayer exciton Bohr radius ($\sim 2 \text{ nm}$) [18]. A desirable property of these quantum emitters is that their energy can be tuned by more than 100 times their linewidth. Thus, we can conclude that localized interlayer excitons are excellent candidates to study dipolar interactions in 2D layered materials.

Having established that we have observed localized interlayer exciton with an out-of-plane dipole, we investigate their dipole-dipole interactions. To this end, we slightly increase the excitation laser power for larger density of excitons. Fig. 3a is the time-trace PL emission of two peaks at ~ 1360 and ~ 1362 meV which show the same spectral jittering pattern, as highlighted by white arrows and dotted circles. This behavior suggests that the two peaks belong to the same localized interlayer exciton. Similar feature is also observed in other localized interlayer excitons, with energy spacing between the two peaks varying from 1 to 5 meV (Fig. 3b and supplementary). We notice that such synchronized spectral jittering is not shown by all the peaks in our collection spot-size. For example, the lowest-energy peak in Fig. 3b exhibits a different pattern. In localized intralayer excitons, a doublet peak structure showing similar synchronized jittering is seen and arises from electron-hole (e-h) exchange interaction which causes a fine structure splitting [18]. However, we can rule out the possibility of such fine structure splitting, as the e-h exchange interaction is strongly quenched in interlayer exciton due to the separation of carriers into distinct layers. Thus, exciton complexes such as charged exciton and biexciton could be the possible origin of the two peak structure.

Excitation power-dependence of emission intensity is an ideal technique to distinguish between charged exciton and biexciton. Fig. 3c-e shows PL spectra at different incident powers. At the lowest power, we only observe the red peak. As the power is increased, the blue peak starts to show up at intermediate power and becomes stronger than the red peak at higher power. This strongly suggests that the blue peak is possibly a biexciton. We thus assign the two peaks as IX and IXX, respectively. We further plot the integrated intensity of each emission peak as a function of excitation power, and fit the data with a power law function, $I \propto P^\alpha$ (Supplementary). The red peak IX2 exhibits a power-law behavior with $\alpha \sim 1.0$, and the blue peak IXX2 shows a super-linear power dependence with $I \propto P^{2\alpha}$. The super-linear power dependence is consistent with our assignment that the blue peak is a biexciton although the confidence in the value of α is poor due to a limited range of powers where the peaks can be observed prior to saturation of their emission intensities. Fig. 3f shows that interlayer exciton and biexciton exhibiting the same E -tuning rate of ~ 310 meV nm V^{-1} suggesting that they both carry a dipole moment.

While the biexciton in monolayer WSe₂ emits at lower energy from PL spectroscopy because of a finite, positive binding energy [27], the energy of interlayer biexciton state is raised up by U_{dd} due to dipolar repulsion (Fig. 4a). Emission from biexciton is thus blue-shifted with respect

to exciton (Fig. 3 and Supplementary). The different energy spacing (1-5 meV) between exciton and biexciton indicates that the dipolar interaction varies among different localized interlayer excitons. As the dipole moment can be assumed to be constant given by the separation of 0.7 nm between the two monolayers, variation in U_{dd} must arise from difference in confinement lengths and consequently interexcitonic distances. To estimate the confinement length from U_{dd} , we assume that the interlayer excitons are confined in a harmonic trap with a width larger than the excitonic Bohr radius such that the dipoles can be treated as point particles without considering their internal structure. As the trap is loaded with an additional exciton, the center-of-mass (COM) wavefunction of each exciton is squeezed to avoid overlap and lower the dipolar repulsion. The modified COM wavefunction of each exciton is no longer that of the ground state but has weight from higher energy excited states. This results in the increase of kinetic energy of the two-particle system. The interexcitonic distance can then be calculated by minimizing the total energy which includes $U_{dd} = p^2/(\epsilon_r r_{ex}^3)$. For an energy difference of 2 meV between the exciton ($|IX\rangle \rightarrow |0\rangle$) and biexciton ($|IXX\rangle \rightarrow |IX\rangle$) emission peaks, we obtain a confinement length of ~ 5 nm which is larger than the Bohr radius, validating our assumption (see Supplementary). We remark that one of the peak from another group shows power dependence with $I \propto P^{3\alpha}$, and possibly corresponds a triexciton. Indeed, at higher incident power, new peaks appear at even higher energy compared to the biexciton peak. We assign them to multi-exciton complexes with a regular arrangement of excitons resembling dipolar lattice, which reduces dipolar repulsion [1] (see Supplementary).

In addition to U_{dd} , depending on the species of biexciton i.e., same valley (X_+X_+ or X_-X_-) or opposite valley (X_+X_-) interlayer excitons, exchange interaction, U_{ex} , should affect the energy of biexciton as well. Here, X_{\pm} denotes the exciton with electron and hole in the $\pm K$ valley. The overall wavefunction of the two-exciton state is antisymmetric in the spatial coordinates to reduce the dipolar repulsion. The bosonic nature of the exciton then implies that the singlet arrangement of spin-valley or the opposite valley biexciton X_+X_- has lower energy whereas the same valley excitons $X_{\pm}X_{\pm}$ have energy further increased by U_{ex} .

Much like the intralayer excitons, the interlayer excitons X_{\pm} couple to circularly-polarized light with opposite helicity (σ^{\pm}) following the optical selection rule [6, 30]. As we only observe one extra peak appearing with larger power, we tentatively suppose this peak is the lower energy X_+X_- biexciton rather than the degenerate X_+X_+ and X_-X_- . U_{ex} needs to be overcome for the observation of X_+X_+ and X_-X_- while the emission in PL typically arises only from the lowest

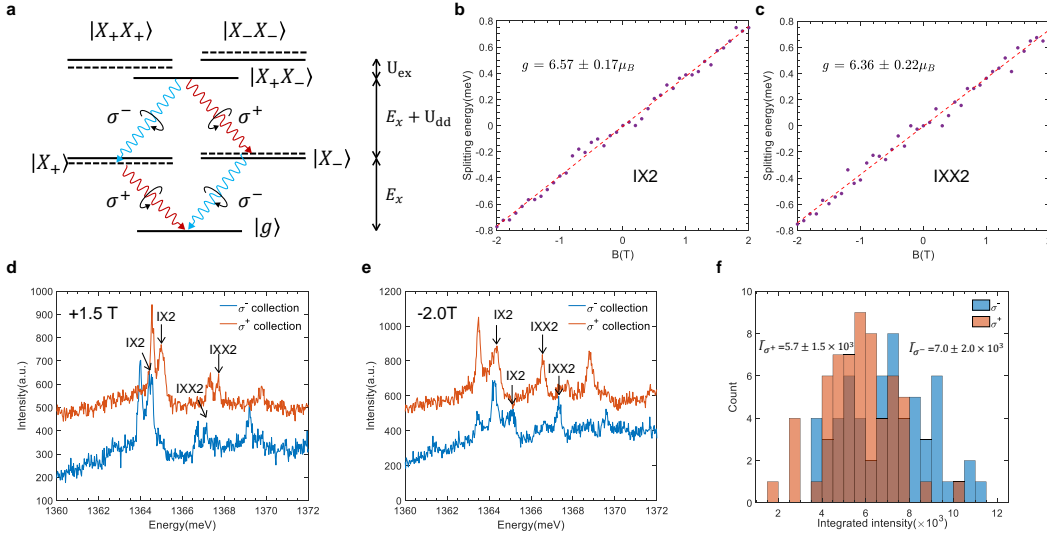


Figure 4: Magnetic field dependence of localized interlayer excitons and biexcitons. **a**, Optical selection rule of IX and IXX under magnetic field. $|X_+\rangle$ and $|X_-\rangle$ states, as well as $|X_+X_+\rangle$ and $|X_-X_- \rangle$, are doubly-degenerate at zero magnetic field, B (solid lines). Lifted degeneracy of $|X_+\rangle$ and $|X_-\rangle$ under finite B (dashed lines) leads to the splitting of $|X_+X_- \rangle$ emission. Red (Blue) peaks of exciton and biexciton are both σ^+ (σ^-) polarized. Degeneracy of $|X_+X_+\rangle$ and $|X_-X_- \rangle$ is also broken under B . **b,c**, B -dependent splitting energies of IX2 (**b**) and IXX2 (**c**). Exciton and biexciton exhibit the same value of g -factor, ~ 6.5 . **d,e**, Polarization-resolved PL spectra of IX2 and IXX2 at +1.5 T(**d**) and -2.0 T(**e**). Polarization of the biexciton peaks follows that of the exciton. **f**, Histogram of biexciton intensity under σ^+ and σ^- excitation configurations at -0.5 T. Biexciton is stronger under σ^- excitation, consistent with the fact that the DCP of exciton is lower when being excited with σ^- polarized light (see Supplementary Information). Excitation wavelength $\lambda = 745$ nm in panel **b-f**. Incident power $P = 250$ nW (linearly-polarized) in panel **b-e**, $P = 150$ nW (circularly-polarized) in panel **f**.

energy state. In other words, if the same valley biexciton is observed in PL emission, one expects to observe X_+X_- simultaneously at the red side of the degenerate X_+X_+ and X_-X_- states which does not seem to be case. The degeneracy of X_+X_+ and X_-X_- , as well as X_+ and X_- , is lifted under finite magnetic field, B (dashed line in Fig. 4a). As illustrated in Fig. 4a, the degeneracy lifting of exciton states causes the PL emission from X_+X_- split into two peaks, though X_+X_- state is hardly affected under B . Co-polarized emission is expected with all red (blue) peaks emitting σ^+ (σ^-) polarized light, as shown in the schematic of Fig. 4a. The situation in Fig. 4a should be contrasted with that of intralayer biexciton where a finite e-h exchange splits the degeneracy of

$X_{\pm}X_{\mp}$ states to make them linearly polarized. As a result, the biexciton cascade of the intralayer exciton yields maximally polarization entangled pairs of photons but the time averaged fidelity of the entanglement is reduced due the e-h splitting [27, 31]. Due to the absence of e-h exchange in interlayer excitons, localized interlayer biexcitons are ideal sources of maximally entangled photons. While the emission rate of our localized interlayer excitons (20 counts/s, see Methods) is slightly larger than the previously reported values [22], it is still too weak to detect entangled photons in a photon coincidence measurement. Recently, layer-hybridized interlayer excitons were reported in vdW heterobilayers where one of the charge carriers is delocalized in both layers thereby increasing the oscillator strength [32, 33].

Next, we proceed to analyze IXs and IXXs under B . Fig. 4b & 4c shows that the IX2 and IXX2 have the same g -factor of ~ 6.5 (also see Supplementary for another quantum emitter group), which implies that the addition of second exciton has negligible impact on the wavefunction corresponding to the relative motion of electrons and holes. This is not surprising because the interlayer exciton Bohr radius (~ 2 nm) is estimated to be the smaller length scale compared to confinement length of the trap (~ 5 nm). As a result, the two excitons in the trap would avoid spatial overlap to reduce U_{dd} without changing the relative motion of the constituent electron-hole pair which determines the g -factor. From polarization-resolved PL measurements (Fig. 4d & 4e), we observe that both red and blue peaks of IXX2 are co-polarized with those of IX2, consistent with the energy diagram in Fig. 4a. To further confirm that the biexciton peak corresponds to a spin-valley singlet configuration as in X_+X_-/X_-X_+ , we analyze the intensity of emission of the two circularly polarized components. A polarization resolved coincidence measurement of the red and blue photons in the biexciton cascade emission unequivocally determines the spin-valley configuration biexciton state. However, this measurement is made difficult due to the weak emission and unsuitable wavelength range for detection with silicon avalanche photodiodes.

In principle, the intensity of X_+X_- ($I_{X_+X_-}$) should depend on the product $I_{X_+} I_{X_-}$, and $I_{X_+X_+}$ ($I_{X_-X_-}$) would be higher if $I_{X_+} I_{X_+}$ ($I_{X_-} I_{X_-}$) is larger. We use excitation polarization to control the degree of circular polarization (DCP) of exciton, such that the relative intensity between X_+ and X_- is modulated while keeping the total intensity unchanged. DCP is obtained by calculating $(I_{\sigma^+} - I_{\sigma^-}) / (I_{\sigma^+} + I_{\sigma^-})$, where a positive (negative) value means the peak is σ^+ (σ^-) polarized. DCP of exciton IX2 under σ^- and σ^+ excitations is -0.19 and -0.29 at $B = -0.5$ T, respectively. Because the exciton is less circularly-polarized with σ^- pumping, we expect IXX2

to be stronger if it is X_+X_- . Histogram based on more than 50 polarization-resolved spectra for each polarization confirms our analysis. Fig. 4f shows that the mean integrated intensity from σ^- excitation is ~ 7000 , and that from σ^+ excitation is only ~ 5700 . To further support our assignment, we calculate the ratio of $I_{XX} / I_{X_+} I_{X_-}$, $I_{XX} / I_{X_+} I_{X_+}$ and $I_{XX} / I_{X_-} I_{X_-}$ (Supplementary Table I). For X_+X_- biexciton, I_{XX} should be proportional to $I_{X_+} I_{X_-}$, regardless of the exciton polarization. However, such a proportionality does not hold for $I_{XX} / I_{X_+} I_{X_+}$ and $I_{XX} / I_{X_-} I_{X_-}$, confirming our assumption. We characterize the difference of ratio (R) between σ^+ and σ^- excitations by calculating $2(R(\sigma^+) - R(\sigma^-)) / (R(\sigma^+) + R(\sigma^-))$. The difference of ratio is one order small for $I_{XX} / I_{X_+} I_{X_-}$ compared to that of $I_{XX} / I_{X_+} I_{X_+}$ and $I_{XX} / I_{X_-} I_{X_-}$ (Supplementary Table I), which is consistent with our assignment that IXX2 is a X_+X_- biexciton.

Although expected, single photon emission was not demonstrated here due to weak emission. Future experiments incorporating localized interlayer excitons in plasmonic nanocavities should be able to enhance the emission rate, as was recently demonstrated for monolayer quantum emitters [34]. Thus, localized interlayer excitons with finite dipole moment constitute quantum emitters with field tuneable energy over a wide range. Moreover, their biexciton cascade emission is devoid of the fine structure splitting which limits the entanglement fidelity of the emitted photon pair in intralayer excitons. In addition, due to their static dipole moment, electrostatic confinement seems to be the natural way to realize an array of quantum emitters with the on-site dipole repulsion leading to the Mott-phase of the Bose-Hubbard model [3, 6]. Another interesting possibility is to confine many dipolar excitons in a larger trap (tens of nm). With increasing exciton density a crystallization phase transition into 1D or 2D dipolar crystal might occur, which could be probed through their phonon modes [14]. A dipolar crystal of an interlayer excitonic condensate might give rise to more exotic many-body states such as supersolids while the internal spin-valley degree of freedom could lead to magnetic instabilities and frustration.

Acknowledgments We acknowledge many enlightening discussions with Ata Imamoğlu and Martin Kroner. We also thank Robert Lemasters and Hayk Harutyunyan for help on atomic layer deposition. A. S. acknowledges support from NSF through the EFRI program-grant # EFMA-1741691.

Author Contributions [†] W. L. and X. L. contributed equally to this work. A. S., W. L., X.

L. and S. D. conceived the project. W. L., X. L., S. D. and L. D. carried out the measurements. W. L. performed the theoretical calculations. X. L., S. D. and L. D. prepared the samples. A. S. supervised the project. All authors were involved in analysis of the experimental data and contributed extensively to this work.

-
- [1] Birnbaum, K. M. *et al.* Photon blockade in an optical cavity with one trapped atom. *Nature* **436**, 87 (2005).
 - [2] Faraon, A. *et al.* Coherent generation of non-classical light on a chip via photon-induced tunnelling and blockade. *Nature Physics* **4**, 859 (2008).
 - [3] Imamoglu, A., Schmidt, H., Woods, G. & Deutsch, M. Strongly interacting photons in a nonlinear cavity. *Phys. Rev. Lett.* **79**, 1467–1470 (1997).
 - [4] Chang, D. E., Vuletić, V. & Lukin, M. D. Quantum nonlinear optics photon by photon. *Nature Photonics* **8**, 685 (2014).
 - [5] Carusotto, I. & Ciuti, C. Quantum fluids of light. *Rev. Mod. Phys.* **85**, 299–366 (2013).
 - [6] Chang, D. *et al.* Crystallization of strongly interacting photons in a nonlinear optical fibre. *Nature physics* **4**, 884 (2008).
 - [7] Lukin, M. *et al.* Dipole blockade and quantum information processing in mesoscopic atomic ensembles. *Physical review letters* **87**, 037901 (2001).
 - [8] Chernikov, A. *et al.* Exciton binding energy and nonhydrogenic rydberg series in monolayer ws_2 . *Phys. Rev. Lett.* **113**, 076802 (2014).
 - [9] He, K. *et al.* Tightly bound excitons in monolayer WSe_2 . *Phys. Rev. Lett.* **113**, 026803 (2014).
 - [10] Rivera, P. *et al.* Observation of long-lived interlayer excitons in monolayer mose_2 – wse_2 heterostructures. *Nature Communications* **6**, 6242 EP – (2015).
 - [11] Tran, K. *et al.* Evidence for moiré excitons in van der waals heterostructures. *Nature* **567**, 71–75 (2019).
 - [12] Rivera, P. *et al.* Valley-polarized exciton dynamics in a 2d semiconductor heterostructure. *Science* **351**, 688–691 (2016).
 - [13] Fogler, M. M., Butov, L. V. & Novoselov, K. S. High-temperature superfluidity with indirect excitons in van der waals heterostructures. *Nature Communications* **5**, 4555 EP – (2014).
 - [14] Rabl, P. & Zoller, P. Molecular dipolar crystals as high-fidelity quantum memory for hybrid quantum computing. *Physical Review A* **76**, 042308 (2007).
 - [15] Lahaye, T., Menotti, C., Santos, L., Lewenstein, M. & Pfau, T. The physics of dipolar bosonic quantum

- gases. *Reports on Progress in Physics* **72**, 126401 (2009).
- [16] Ciarrocchi, A. *et al.* Polarization switching and electrical control of interlayer excitons in two-dimensional van der waals heterostructures. *Nature photonics* **13**, 131–136 (2019).
 - [17] Nagler, P. *et al.* Interlayer exciton dynamics in a dichalcogenide monolayer heterostructure. *2D Materials* **4**, 025112 (2017).
 - [18] Atatüre, M., Englund, D., Vamivakas, N., Lee, S.-Y. & Wrachtrup, J. Material platforms for spin-based photonic quantum technologies. *Nature Reviews Materials* **3**, 38 (2018).
 - [19] Aharonovich, I., Englund, D. & Toth, M. Solid-state single-photon emitters. *Nature Photonics* **10**, 631 EP – (2016).
 - [20] Lu, X. *et al.* Optical initialization of a single spin-valley in charged wse₂ quantum dots. *Nature nanotechnology* (2019).
 - [21] Brotons-Gisbert, M. *et al.* Coulomb blockade in an atomically thin quantum dot coupled to a tunable fermi reservoir. *Nature nanotechnology* **14**, 442 (2019).
 - [22] Seyler, K. L. *et al.* Signatures of moiré-trapped valley excitons in mose₂/wse₂ heterobilayers. *Nature* **567**, 66 (2019).
 - [23] Saffman, M., Walker, T. G. & Mølmer, K. Quantum information with rydberg atoms. *Rev. Mod. Phys.* **82**, 2313–2363 (2010).
 - [24] Rivera, P. *et al.* Interlayer valley excitons in heterobilayers of transition metal dichalcogenides. *Nature nanotechnology* **13**, 1004–1015 (2018).
 - [25] Schaibley, J. R. *et al.* Directional interlayer spin-valley transfer in two-dimensional heterostructures. *Nature Communications* **7**, 13747 EP – (2016).
 - [26] Branny, A. *et al.* Discrete quantum dot like emitters in monolayer mose₂: Spatial mapping, magneto-optics, and charge tuning. *Applied Physics Letters* **108**, 142101 (2016).
 - [27] He, Y.-M. *et al.* Cascaded emission of single photons from the biexciton in monolayered wse₂. *Nature Communications* **7**, 13409 (2016). URL <http://dx.doi.org/10.1038/ncomms13409>. Article.
 - [28] Schinner, G. J. *et al.* Confinement and interaction of single indirect excitons in a voltage-controlled trap formed inside double ingaas quantum wells. *Phys. Rev. Lett.* **110**, 127403 (2013).
 - [29] Yu, H., Liu, G.-B., Tang, J., Xu, X. & Yao, W. Moiré excitons: From programmable quantum emitter arrays to spin-orbit-coupled artificial lattices. *Science Advances* **3** (2017).
 - [30] Wu, F., Lovorn, T. & MacDonald, A. Theory of optical absorption by interlayer excitons in transition metal dichalcogenide heterobilayers. *Physical Review B* **97**, 035306 (2018).
 - [31] Huber, D. *et al.* Strain-tunable gaas quantum dot: A nearly dephasing-free source of entangled photon pairs on demand. *Phys. Rev. Lett.* **121**, 033902 (2018).
 - [32] Alexeev, E. M. *et al.* Resonantly hybridized excitons in moiré superlattices in van der waals heterostructures. *Nature* **567**, 81–86 (2019).

- [33] Hsu, W.-T. *et al.* Tailoring excitonic states of van der waals bilayers through stacking configuration, band alignment and valley-spin. *arXiv preprint arXiv:1903.02157* (2019).
- [34] Luo, Y. *et al.* Deterministic coupling of site-controlled quantum emitters in monolayer wse2 to plasmonic nanocavities. *Nature Nanotechnology* (2018).
- [35] Wu, F., Lovorn, T., Tutuc, E. & MacDonald, A. H. Hubbard model physics in transition metal dichalcogenide moiré bands. *Phys. Rev. Lett.* **121**, 026402 (2018).

Methods

Sample fabrication We use electron beam lithography and thermal evaporator to fabricate the pillar arrays (5 nmCr/85 nmAu) or electrical contacts (5 nmCr/55 nmAu) on 300 nm SiO₂/Si substrate. A thin layer of SiO₂ (3 nm) is subsequently deposited on pillars by using atomic layer deposition as the spacer. We transfer the mechanically exfoliated samples by polydimethylsiloxane-based dry transfer method on the as-patterned pillars/electrical contacts, with monolayer WSe₂ (HQ graphene) on top of monolayer MoSe₂ (HQ graphene). The sample with electrical contacts is encapsulated between two hexagonal boron nitride (HQ graphene) layers. Graphite (NGS) layers are used as the bottom gate and top gates. After the stacking of top MoSe₂, the sample is annealed in 5% H₂/95% N₂ at 125°C for 2 h.

Photoluminescence spectroscopy Photoluminescence spectroscopy is based on two home-built low temperature microscope set-ups. The WSe₂/MoSe₂ sample is loaded into a closed-cycle cryostat (AttoDry 800) with the electrical connection and then into another cryostat (BlueFors cryogenics) with magnetic field from -8 T to +8 T. Both of them are cooled to ~ 4 K all conducted measurements. A piezoelectric controller (Attocube systems) is used to position the sample. The emission is collected using an achromatic lens (NA = 0.42 for AttoDry 800 and NA = 0.63 for BlueFors cryogenics) and directed to a high-resolution (focal length: 500 mm for AttoDry 800 and 750 mm for BlueFors cryogenics) spectrometer (Princeton Instrument HR-500 for AttoDry 800 and Princeton Instruments SP-2750 for BlueFors cryogenics) where it is dispersed by a 1200 g/mm or 300 g/m grating (both blazed at 750 nm). A charge coupled device (Princeton Instrument PIXIS-400 CCD for AttoDry 800 and PyLoN CCD for BlueFors cryogenics) is used as a detector. The excitation laser is a mode-hop-free tunable continuous-wave Ti:Sapphire laser (MSquared Lasers) with resolution of 0.1 pm are coupled to a single-mode fiber to clean the mode. The Ti:Sapphire laser has spot size of $\sim 1\mu\text{m}$. The polarization of the incident laser is controlled using a polarizer together with a liquid crystal variable retarder (LCR). The polarization detection is performed by using

a $\lambda/4$ waveplate (achromatic, 690-1200 nm) placed before the Wollaston prism. The circularly polarized emission is converted into linearly polarized light through the $\lambda/4$ waveplate. The s- and p- components of linear polarized light is then displaced by the Wollaston prism. Another achromatic $\lambda/4$ waveplate is placed after the Wollaston prism to convert the linearly polarized light into a circularly polarized signal, in order to avoid the sensitivity to the grating efficiency. In all measurements, the magnetic field B is applied perpendicular to the plane of the sample and the voltage is applied to the graphite gates with a Keithley 2400 sourcemeter.

Supplementary Information Contents:

Figure S1. Time-trace photoluminescence (PL) emission of localized interlayer excitons.

Figure S2. Linewidths from from localized interlayer excitons.

Figure S3. Electrical tuning of IX3 group.

Figure S4. PL of IX3 group under different excitation powers.

Figure S5. Localized interlayer exciton IX4 and biexciton IXX4.

Figure S6. Power dependence of localized interlayer excitons and biexcitons.

Figure S7. Multi-excitonic complex of localized interlayer excitons.

Figure S8. PL of localized interlayer exciton IX5 group under different excitation powers.

Figure S9. g -factors of localized interlayer excitons in IX5 group.

Table I. Correlation of biexciton and exciton intensities for IX2-IXX2.

Note 1. Estimation of confinement length for exciton IX.

Note 2. Estimation of exchange energy for biexciton IXX.

Note 3. Estimation of total energy of triexciton IXXX.

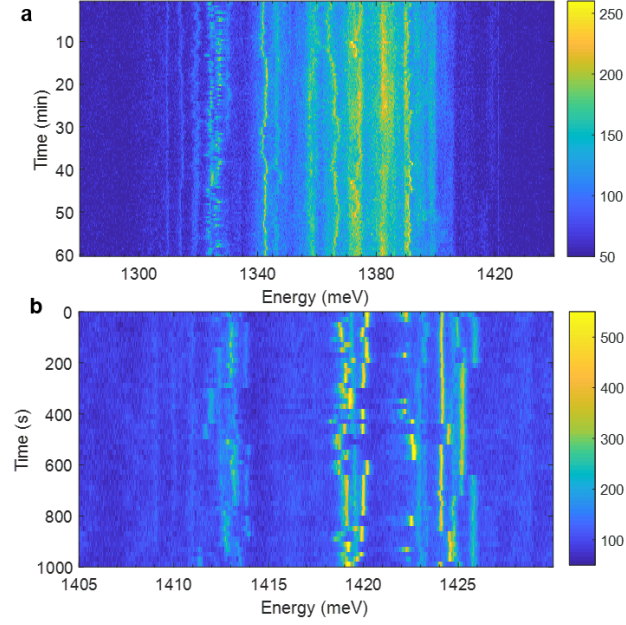


Figure S1: Time-trace PL emission of localized interlayer excitons in $\text{MoSe}_2/\text{WSe}_2$ heterostructure. Sharp peaks spectrally wander in the range of 1300 to 1430 meV, indicating that they are originating from interlayer excitons. Excitation is linearly-polarized, with wavelength $\lambda = 740$ nm in panel **a**, $\lambda = 735$ nm in panel **b**. Incident power $P = 30$ nW in panel **a**, $P = 20$ nW in panel **b**.

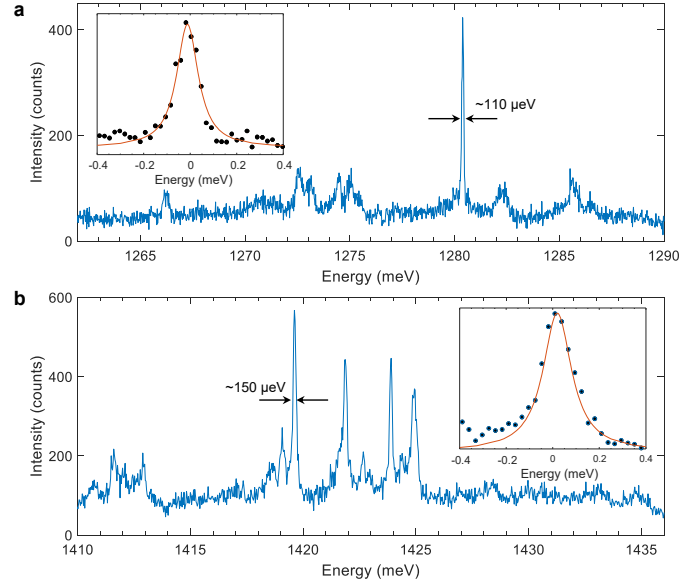


Figure S2: Linewidths from localized interlayer excitons. PL spectra of localized interlayer excitons showing sharp linewidths of $\sim 110 \mu\text{eV}$ (a) and $\sim 150 \mu\text{eV}$ (b). Inset: fitting with Lorentzian function for localized interlayer excitons at $\sim 1280 \text{ meV}$ (a) and $\sim 1420 \text{ meV}$ (b). Excitation is linearly-polarized, with wavelength $\lambda = 770 \text{ nm}$ in panel **a**, $\lambda = 735 \text{ nm}$ in panel **b**. Incident power $P = 6.5 \text{ nW}$ in panel **a**, $P = 20 \text{ nW}$ in panel **b**.

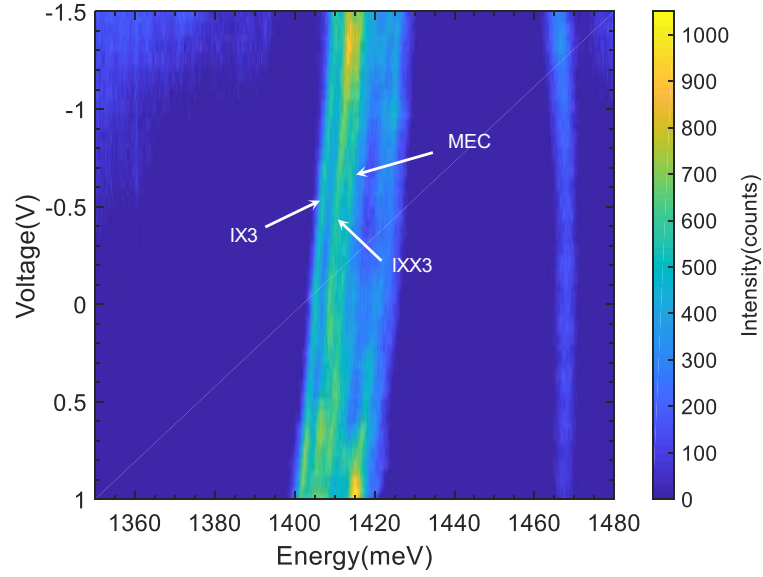


Figure S3: Electrical tuning of IX3 group. Exciton IX3, biexciton IXX3 and multi-excitonic complex (MEC) show the same tuning rate as bottom gate voltage changes from -1.5 V to +1 V. Excitation is linearly-polarized, with wavelength $\lambda = 758$ nm. Incident power $P = 8 \mu\text{W}$.

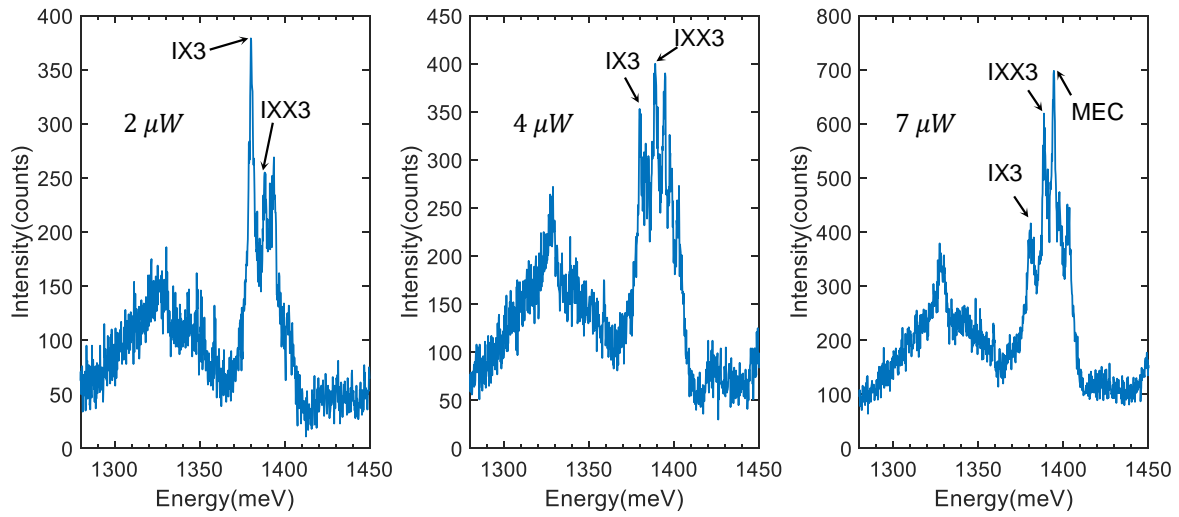


Figure S4: PL spectra of IX3 group under different excitation powers. At low power $P = 2 \mu\text{W}$, exciton IX3 is stronger than biexciton IXX3 (left). IXX3 is stronger than IX3 when $P = 4 \mu\text{W}$ (middle). MEC appears and dominates when $P = 7 \mu\text{W}$ (right). Excitation is linearly-polarized, with wavelength $\lambda = 765$ nm.

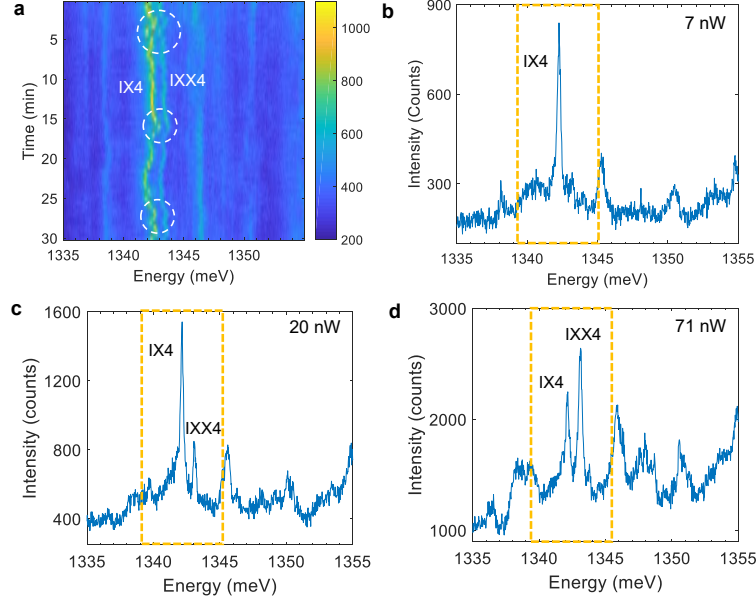


Figure S5: Localized interlayer exciton IX4 and biexciton IXX4. **a**, Time-trace PL emission of interlayer exciton IX4 and biexciton IXX4. Dashed circles highlight the same spectral jittering patterns, which implies that IX4 and IXX4 are correlated. **b-d** PL spectra of IX4-IXX4 under different excitation powers, 7 nW (**b**), 20 nW (**c**) and 71 nW (**d**). Only exciton IX4 appears at low power (7 nW). Biexciton IXX4 shows up at intermediate power (20 nW) and becomes stronger than IX4 at high power (71 nW). Excitation laser is linearly-polarized, with wavelength $\lambda = 745$ nm. Incident power $P = 50$ nW in panel **a**.

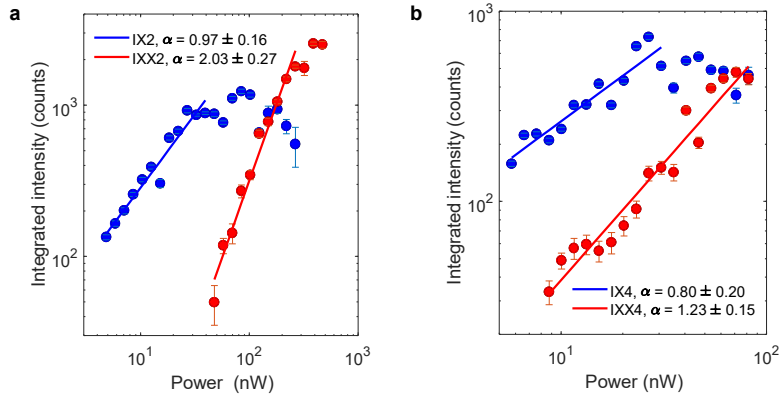


Figure S6: Power-dependence of localized interlayer excitons and biexcitons. Integrated intensity of emission peaks in IX2-IXX2 (**a**) and IX4-IXX4 (**b**). The fitting was done with a power law function, $I \propto P^\alpha$. We obtain $\alpha(IXX) \approx 2\alpha(IX)$, indicating that IXX2 and IXX4 are biexcitons.

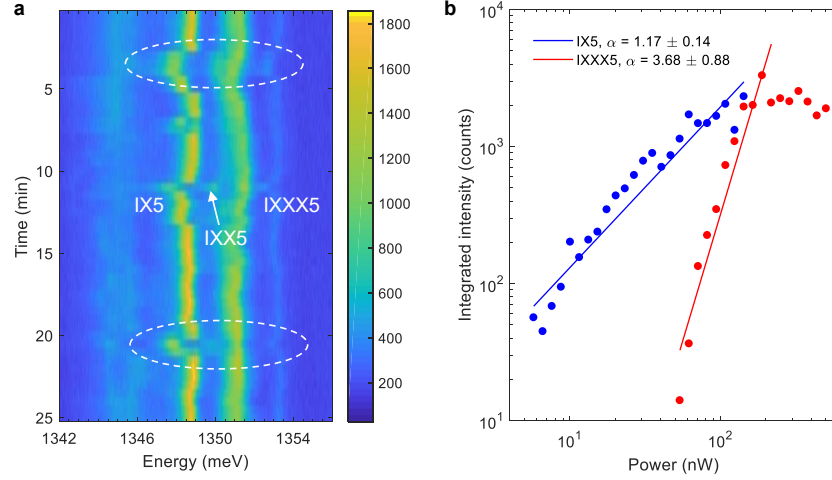


Figure S7: Multi-excitonic complex of localized interlayer excitons. **a**, Time-trace PL emission of interlayer exciton IX5, biexciton IXX5 and triexciton IXXX5. Dashed circles highlight the same spectral jittering patterns. Energy spacings between IX5 & IXX5 and IX5 & IXXX5 are ~ 2.3 meV and ~ 4.7 meV, respectively. **b**, Integrated intensity of emission peaks IX5 and IXXX5. We obtain $\alpha(\text{IXXX5}) \approx 3\alpha(\text{IX})$ from power-law fitting, indicating that IXXX5 is a triexciton. As the emission energy of IXX5 is very close to another uncorrelated and strong peak (shown in a), we can not extract the power-dependent integrated intensity for IXX5. Excitation is linearly-polarized, with wavelength $\lambda = 725$ nm in panel **a**, $\lambda = 745$ nm in panel **b**. Incident power $P = 45$ nW in panel **a**.

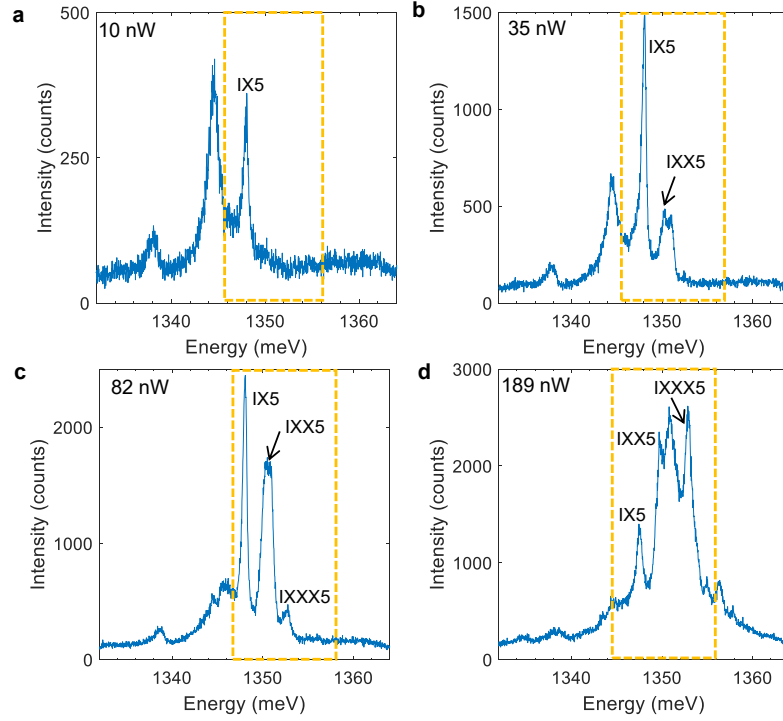


Figure S8: PL emission of interlayer exciton IX5 group under difference excitation powers.

Only exciton IX5 shows up at low power, 10 nW(a). Biexciton IX5 starts to appear at $P = 35$ nW (b), and triexciton IXXX5 is activated at higher power 82 nW (c). At $P = 189$ nW (d), triexciton IXXX5 is stronger than biexciton IXX5, and exciton IX5 is the weakest. Excitation is linearly-polarized, with wavelength $\lambda = 745$ nm.

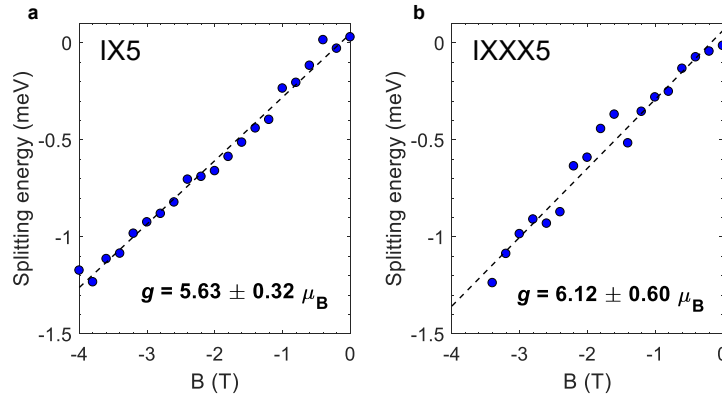


Figure S9: g -factors of localized interlayer excitons in IX5 group. Exciton IX5 (a) and triexciton IXXX5 (b) exhibit the same value of g -factor. Excitation is linearly-polarized, with wavelength $\lambda = 745$ nm. Incident power $P = 180$ nW.

Table I: Correlation of biexciton and exciton intensities for IX2-IXX2

	σ^- excitation	σ^+ excitation	Difference ²
DCP of exciton ¹	-0.19	-0.29	-0.10
$I_{XX} / I_{X+} I_{X-}$	11.035e-05	10.823e-05	-0.48%
$I_{XX} / I_{X+} I_{X+}$	1.6543e-04	2.0172e-04	4.94%
$I_{XX} / I_{X-} I_{X-}$	7.4878e-05	5.9556e-05	-5.70%

¹ Degree of circular polarization (DCP) of exciton, is obtained by calculating $(I_{\sigma^+} - I_{\sigma^-}) / (I_{\sigma^+} + I_{\sigma^-})$.

² Difference of DCP is calculated by: $\text{DCP}(\sigma^+) - \text{DCP}(\sigma^-)$. Differences of Ratio R , such as R of $I_{XX} / I_{X+} I_{X-}$, is obtained by calculating $2(R(\sigma^+) - R(\sigma^-)) / (R(\sigma^+) + R(\sigma^-))$.

Note 1: Estimation of the confinement length forexciton IX [1]

According to the dipolar-crystal-like model, the overlap of the excitonic wavefunctions is neglected, so the total exciton energy in a parabolic trap is given by

$$E_{NIX} = NE_{IX}^0 + \sum_i \frac{M\Omega^2}{2} r_i^2 + \sum_{i < j, i, j=1, \dots, N} \frac{d^2}{\epsilon_r r_{i,j}^3},$$

where N is the number of excitons, E_{IX}^0 is the optical energy of the exciton, Ω is the characteristic confinement frequency of an exciton in the trap. $M = m_e^* + m_h^*$ is the total exciton mass, d is the interlayer spacing, r_i is the coordinate of i -exciton, and $r_{i,j}$ is the distance between i -, j -exciton. In order to calculate the emission energy of biexciton, we only need to consider the single exciton and biexciton energy

$$E_{IX} = E_{IX}^0 + \frac{M\Omega^2}{2} r_1^2,$$

$$E_{IXX} = 2E_{IX}^0 + \frac{M\Omega^2 r_1^2}{2} + \frac{M\Omega^2 r_2^2}{2} + \frac{d^2}{\epsilon_r r_{1,2}^3}.$$

The emission energy of biexciton is given by

$$\hbar\omega_{IXX} = E_{IXX, \min} - E_{IX, \min},$$

where the $E_{IX, \min}$, $E_{IXX, \min}$ are the minimum of E_{IX} , E_{IXX} , that is, the ground states of IX and IXX respectively. For the exciton IX, the ground state is that the exciton stays at the lowest potential energy; for the biexciton IXX, due to the repulsive onsite dipole-dipole interaction ($U_{\text{dd}}^{\text{on-site}}$)

between two excitons, the ground state is a diatomic geometry with $r_1 = -r_2 = \frac{1}{2}r_{1,2} = R_{IXX}$,

$$E_{IX,\min} = E_{IX}^0,$$

$$E_{IXX,\min} = 2E_{IX}^0 + 2\frac{M\Omega^2 R_{eq,IXX}^2}{2} + \frac{d^2}{8\epsilon_r R_{eq,IXX}^3},$$

where $R_{eq,IXX} = (\frac{3d^2}{16\epsilon_r M\Omega^2})^{\frac{1}{5}}$ is the solution for $\frac{dE_{IXX}}{dR_{IXX}} = 0$. Then we can get

$$\hbar\omega_{IXX} = E_{IX}^0 + [(\frac{3}{16})^{\frac{2}{5}} + (\frac{1}{6})^{\frac{3}{5}}](\frac{M^3\Omega^6 d^4}{\epsilon_r^2})^{\frac{1}{5}}.$$

Therefore, the energy spacing between the IX and IXX emission is $\Delta E = [(\frac{3}{16})^{\frac{2}{5}} + (\frac{1}{6})^{\frac{3}{5}}](\frac{M^3\Omega^6 d^4}{\epsilon_r^2})^{\frac{1}{5}}$.

In the WSe₂/MoSe₂ heterobilayer, $M = m_e^* + m_h^* \approx 1.15m_0$, where m_0 is the electron bare mass [2, 3], $d = 0.7$ nm [4], $\epsilon_r \approx (1 + 3.9)/2 = 2.45$ [5] for the SiO₂ substrate. Considering the energy spacings ΔE in Fig. 3a & 3b from main text are ~ 2 meV, we obtain the parabolic confinement frequency $\Omega \sim 2.51$ meV. The confinement frequency Ω is related to the confinement length l by $\Omega = \frac{\hbar}{Ml^2}$, so the confinement length for our interlayer quantum emitter is ~ 5.14 nm. The Bohr radius a_B for IX is ~ 2 nm [6], smaller than the confinement length, which validates the model.

Note 2: Estimation of the exchange energy of biexciton IXX [4, 6]

The on-site Coulomb interaction between two IX wavepackets in the same quantum emitter can be separated into two parts: (i) dipole-dipole interaction $U_{dd}^{\text{on-site}}$ regardless of the valley index ($|X_+X_- \rangle$, $|X_+X_+ \rangle$ and $|X_-X_- \rangle$),

$$U_{dd}^{\text{on-site}} = \frac{1}{2\pi}(\frac{a_B}{w})^2 \frac{d}{a_B} E_b,$$

(ii) Exchange interaction U_{ex} between excitons in the same valley only ($|X_+X_+ \rangle$ and $|X_-X_- \rangle$),

$$U_{ex} = \frac{1}{2\pi}(\frac{a_B}{w})^2 E_b,$$

where a_B is the exciton Bohr radius, w is the real space extension of the exciton center of mass wavefunction, E_b is the interlayer exciton binding energy. The energy spacing between IXX and IX in the main text is actually $U_{dd}^{\text{on-site}}$ of 2.0 meV, since no exchange interaction exists in $|X_+X_- \rangle$. Using $E_b = 0.2$ eV, $a_B = 2$ nm, we have $w \sim 4.7$ nm, $U_{ex} \sim 5.7$ meV. Large U_{ex} makes the $|X_+X_+ \rangle$ or $|X_-X_- \rangle$ have much higher energy than $|X_+X_- \rangle$ and not favorable due to thermalization.

Note 3: Estimation of total energy of triexciton IXXX [1]

Let us use the above model to consider the transition from $|X_+X_+X_- \rangle$ (or $|X_-X_-X_+ \rangle$) to $|X_+X_- \rangle$ and then from $|X_+X_- \rangle$ to either $|X_+ \rangle$ or $|X_- \rangle$. The exciton energy is

$$E_{IX,min} = E_{IX}^0,$$

The biexciton energy is

$$E_{IXX,min} = 2E_{IX}^0 + U_{dd,2} = 2E_{IX}^0 + 2.3meV,$$

and the triexciton energy is

$$\begin{aligned} E_{IXXX,min} &= 3E_{IX}^0 + 3U_{dd,3} + U_{ex} = 3E_{IX}^0 + 3\frac{M\Omega^2 r_{eq,3}^2}{2} + \frac{\sqrt{3}e^2 d^2}{3\epsilon r_{eq,3}^3} + U_{ex} \\ &= 3E_{IX}^0 + 5.4meV + U_{ex, req,3} = \left(\frac{\sqrt{3}e^2 d^2}{3\epsilon M\Omega^2}\right)^{\frac{1}{5}}, \end{aligned}$$

where $U_{dd,2}$ is the dipole-dipole interaction at the biexciton states IXX with a diatomic geometry, which is from the experiment and gives the value of Ω . $U_{dd,3}$ is the calculated dipole-dipole interaction between each two exciton at the triexciton states IXXX with a symmetric triangular geometry, and U_{ex} is the exchange energy between the two dipoles in the same valley. Here we ignore the reorganization of the IXXX by the exchange energy.

If $U_{ex} = 0$, we can get the lower bound of $E_{IXXX,min}$ to be $3E_{IX}^0 + 5.4$ meV; if we use the same relation between U_{ex} and U_{dd} as in the biexciton states, which is $U_{ex} = \frac{a_B}{d} U_{dd,3} = \frac{2}{0.7} \frac{5.4}{3} = 5.14$ meV with $a_B = 2$ nm and $d = 0.7$ nm, the higher bound of $E_{IXXX,min}$ is estimated to be $3E_{IX}^0 + 10.54$ meV.

In the experiment spectra with IX5, IXX5, and IXXX5,

$$E_{IXX,min} - E_{IX,min} = \hbar\omega_{IXX} = E_{IX}^0 + 2.3meV,$$

$$E_{IXXX,min} - E_{IXX,min} = \hbar\omega_{IXXX} = E_{IX}^0 + 4.7meV,$$

Adding the two equations, we have the experiment result is $E_{IXXX,min} = 3E_{IX}^0 + 7.0$ meV, within the estimated range.

If we consider the reorganization, IXXX becomes an asymmetric configuration to lower the total energy of IXXX, which could match the experiment result. In other words, the estimation

of $U_{ex} = \frac{a_B}{d} U_{dd,3}$ is resonable.

-
- [1] Schinner, G. J. *et al.* Confinement and interaction of single indirect excitons in a voltage-controlled trap formed inside double in GaAs quantum wells. *Phys. Rev. Lett.* **110**, 127403 (2013).
 - [2] Larentis, S. *et al.* Large effective mass and interaction-enhanced zeeman splitting of k-valley electrons in MoSe₂. *Phys. Rev. B* **97**, 201407 (2018).
 - [3] Wu, F., Lovorn, T., Tutuc, E. & MacDonald, A. H. Hubbard model physics in transition metal dichalcogenide moiré bands. *Phys. Rev. Lett.* **121**, 026402 (2018).
 - [4] Rivera, P. *et al.* Valley-polarized exciton dynamics in a 2D semiconductor heterostructure. *Science* **351**, 688–691 (2016).
 - [5] Chernikov, A. *et al.* Exciton binding energy and nonhydrogenic rydberg series in monolayer WS₂. *Phys. Rev. Lett.* **113**, 076802 (2014).
 - [6] Yu, H., Liu, G.-B., Tang, J., Xu, X. & Yao, W. Moiré excitons: From programmable quantum emitter arrays to spin-orbit-coupled artificial lattices. *Sci. Adv.* **3**, e1701696 (2017).